Zhu et al. *Zool. Res.* 2025, 46(5): 1153−1164
https://doi.org/10.24272/j.issn.2095-8137.2025.307
https://cstr.cn/32248.14.zr.2025.307

ZR | Zoological Research

Article Open Access

LEAP2 triggers retromer-mediated membrane trafficking of MOSPD2 to promote chemotaxis in teleost monocytes/macrophages

Ting-Fang Zhu[1,2,3], Zi-Yue Zhao[1,2,3], Chen-Jie Fei[1,2,3], Shi-Chang Shen[2], Jian-Zhong Shao[4], Li Nie[1,2,3,*], Jiong Chen[1,2,3,*]

[1] *State Key Laboratory for Quality and Safety of Agro-Products*, *Ningbo University*, *Ningbo*, *Zhejiang* 315832, *China*

[2] *Laboratory of Biochemistry and Molecular Biology*, *School of Marine Sciences*, *Meishan Campus*, *Ningbo University*, *Ningbo*, *Zhejiang* 315832, *China*

[3] *Key Laboratory of Aquacultural Biotechnology of Ministry of Education*, *Ningbo University*, *Ningbo*, *Zhejiang* 315832, *China*

[4] *College of Life Sciences*, *Key Laboratory for Cell and Gene Engineering of Zhejiang Province*, *Zhejiang University*, *Hangzhou*, *Zhejiang* 310058, *China*

ABSTRACT

Liver-expressed antimicrobial peptide 2 (LEAP2) is a key regulator of innate immune defense in teleosts, yet the molecular basis of its chemotactic function remains largely unidentified. *Boleophthalmus pectinirostris* MOSPD2 (*Bp*MOSPD2) was previously identified as a candidate receptor for *Bp*LEAP2 in monocytes/macrophages (MO/MΦ). In the present study, *Bp*LEAP2 stimulation was found to trigger a retromer-dependent intracellular trafficking program essential for *Bp*MOSPD2-mediated chemotaxis. Exposure to *Bp*LEAP2 significantly enhanced *Bp*MO/MΦ migration and promoted the accumulation of *Bp*MOSPD2 at the plasma membrane. Subcellular fractionation and immunofluorescence analyses revealed that *Bp*MOSPD2 translocated from the endoplasmic reticulum (ER) to early endosomes upon *Bp*LEAP2 stimulation, followed by redistribution to the cell surface. Blockade of ER export or knockdown of core retromer subunits (*Bp*VPS35, *Bp*VPS26, or *Bp*VPS29) abolished membrane localization and attenuated *Bp*LEAP2-induced migration. Co-immunoprecipitation combined with mass spectrometry confirmed direct binding between *Bp*MOSPD2 and *Bp*VPS35, while domain-mapping indicated that this interaction was not exclusively dependent on MSP or CRAL-TRIO domains. Depletion of individual retromer components led to retention of *Bp*MOSPD2 in early endosomes, establishing the necessity of the retromer complex for receptor recycling. Functionally, disruption of this complex eliminated the pro-migratory activity of *Bp*LEAP2 on *Bp*MO/MΦ. These findings identify the retromer complex as a critical regulator of *Bp*MOSPD2 trafficking and uncover a previously unrecognized mechanism through which *Bp*LEAP2 promotes MO/MΦ migration in teleosts.

Keywords: LEAP2; MOSPD2; Retromer complex; Membrane trafficking; Chemotaxis

INTRODUCTION

Motile sperm domain-containing protein 2 (MOSPD2) is a single-pass transmembrane protein characterized by an N-terminal CRAL-TRIO domain—originally identified in cellular retinaldehyde-binding protein (CRALBP) and triple functional domain protein (TRIO)—followed by a major sperm protein (MSP) domain and a potential C-terminal transmembrane domain. The MSP domain exhibits structural homology to members of the vesicle-associated membrane protein-associated protein (VAP) family, which localize predominantly to the endoplasmic reticulum (ER) and mediate interorganelle tethering at membrane contact sites (Di Mattia et al., 2018; James & Kehlenbach, 2021; Neefjes & Cabukusta, 2021; Zouiouich et al., 2022). Although initially described as an ER-resident scaffold, MOSPD2 has also been detected at the plasma membrane in monocytes and tumor cells, where it contributes to chemokine-driven migration and metastatic behavior (Mendel et al., 2017; Salem et al., 2019, 2025; Yacov et al., 2020). However, the mechanisms governing this dual subcellular localization, and their relevance to immune signaling, remain poorly defined.

Our previous studies in the mudskipper (*Boleophthalmus pectinirostris*) identified liver-expressed antimicrobial peptide 2 (LEAP2) as an immunoregulatory factor that enhances pathogen clearance and host survival following *Edwardsiella*

Received: 29 July 2025; Accepted: 08 September 2025; Online: 09 September 2025

Foundation items: This work was supported by the National Natural Science Foundation of China (32173004) and Natural Science Foundation of Zhejiang Province (LZ23C190001)

*Corresponding authors, E-mail: nieli@nbu.edu.cn; chenjiong@nbu.edu.cn

tarda infection, despite lacking direct bactericidal activity (Chen et al., 2016). Subsequent work implicated *Bp*MOSPD2 as the receptor mediating LEAP2-driven chemotaxis in monocytes and macrophages (MO/MΦ) (Li et al., 2020). However, the redistribution of MOSPD2 from the ER to the plasma membrane under stimulatory conditions, and the cellular machinery orchestrating this relocation, are yet to be characterized (Di Mattia et al., 2018; Mendel et al., 2017; Salem et al., 2019, 2025; Zouiouich et al., 2022).

The retromer complex, comprising vacuolar protein sorting-associated protein VPS35, VPS26, and VPS29, is an evolutionarily conserved endosomal sorting platform that regulates the retrograde transport and surface recycling of transmembrane cargo from early endosomes to the trans-Golgi network or plasma membrane (Edgar & Polak, 2000; Haft et al., 2000; Seaman et al., 1998; Seaman, 2021; Zhang et al., 2025). Although retromer activity has been linked to immune receptor trafficking, its role in chemotactic peptide signaling within innate immune cells has not been systematically investigated.

This study employed *B. pectinirostris* as a teleost model to dissect the intracellular trafficking events underlying LEAP2-mediated chemotaxis. Notably, *Bp*LEAP2 stimulation induced ER-to-endosome translocation of *Bp*MOSPD2, where it engaged with *Bp*VPS35. This interaction facilitated retromer-dependent delivery of *Bp*MOSPD2 to the cell surface, an essential process for LEAP2-induced macrophage chemotaxis. Overall, these findings delineate a previously unrecognized role for the retromer complex in innate immune signaling and establish a mechanistic link between the dual localizations of MOSPD2 in teleost immune cells.

MATERIALS AND METHODS

Fish rearing

Mudskippers (30–35 g) were obtained from the Lulin aquaculture facility (Ningbo, China). Fish were acclimated in brackish water (10% salinity), maintained at 24–26°C in a recirculating water system for two weeks prior to experiments. All animal procedures were conducted in accordance with the Experimental Animal Management Law of China and were approved by the Animal Ethics Committee of Ningbo University (protocol no. 10071).

Cell isolation and culture

HEK293T and HeLa cells were obtained from the Shanghai Institute of Biochemistry and Cell Biology Cell Bank (https://www.cellbank.org.cn/) and cultured in Dulbecco's modified Eagle's medium (DMEM, #11965092, Thermo Fisher Scientific, USA) supplemented with 10% fetal bovine serum (FBS, #10437, Thermo Fisher Scientific, USA) and 1% penicillin-streptomycin (P/S, #SV30010, HyClone, USA) at 37°C in a 5% CO_2 atmosphere.

*Bp*MO/MΦ cells were isolated as previously described (Nie et al., 2025). Briefly, following tail vein blood collection, renal tissue was extracted and placed in medium I (RPMI 1640 (#11875093, Thermo Fisher Scientific, USA) containing 2% FBS, 1% P/S, and 120 U/mL heparin (#H3149, Sigma-Aldrich, USA)). Kidneys were passed through 100 μm nylon strainers (#352360, Corning Life Sciences, USA), and the resulting cell suspensions were subjected to density gradient centrifugation using Ficoll (#10307793, Cytiva, USA) at a 1:1 ratio. Following centrifugation at 2 500 ×*g* for 25 min at room temperature, the white blood cell layer was carefully collected and further purified by centrifugation with an equal volume of medium I. The resulting cells were further washed with medium II (RPMI 1640 containing 0.1% FBS, 1% P/S, and 120 U/mL heparin) and resuspended in the same medium. Cells were seeded at 2×10^7 cells/mL into 6-well plates and incubated overnight at 24°C with 5% CO_2. The following day, cells were washed three times with RPMI 1640 medium and cultured with complement medium (10% FBS and 1% P/S in RPMI 1640 medium) at 24°C with 5% CO_2 until further experimentation.

Peptides

Custom peptides, including the mature *Bp*LEAP2 peptide (MTPLWRILNSKPFGAYCQNNYECSTGLCRAGFCATMHRSA TVSVTN) and a scrambled control peptide (ILANACT FCGSAAFMCLNNSGESLKCVWRTTTSRPNVRHPTMYQYG), were synthesized by GL Biochem (Shanghai) Ltd. (China).

Plasmid construction

Full-length coding sequences of *BpMOSPD2*, *BpVPS35*, *BpVPS26*, and *BpVPS29* were amplified and inserted into HA- or Flag-tagged pcDNA3.1 vectors using a Seamless Cloning Kit (#CU201, TrasGen Biotech, China). Truncation mutants of *BpMOSPD2* were also generated. All constructs were confirmed by DNA sequencing (Youkang Biotechnology, China). Primer sequences are provided in Supplementary Table S1.

Plasmid transfection

HEK293T cells were transfected with plasmids using polyethylenimine (#49553-93-7, Polysciences Inc., USA), and HeLa cells were transfected using Lipofectamine 3000 (#15338100, Thermo Fisher Scientific, USA).

siRNA interference

Cells were seeded at 2×10^7 cells/well in 6-well plates and transfected with 60 pmol of the indicated siRNA using 18 μL of Lipofectamine RNAimax (#13778150, Thermo Fisher Scientific, USA). All siRNA transfections were performed under identical conditions and allowed to proceed for 48 h prior to subsequent analyses. The siRNA sequences used included: *BpMOSPD2*: 5'-GGACCCGAGGCAATCAGCAAACTCA-3'; *BpVPS35*: 5'-ATCATCGCCCTTATTGACCG-3'; *BpVPS26*: GCCAGTTTGT GAGATAGATGTAC; *BpVPS29*: GGGGAATCTATGCACTAA AGAAA; *hVPS35*: 5'-3': GCCTTCAGAGGATGTTGTATC TTTA; *hVPS26*: 5'-3': GCTAGAACACCAAGGAATT; *hVPS29*: 5'-3': ATGATGTGAAAGTAGAACGAATCGA; and scrambled siRNA: 5'-CCGAACGGACTAAACACTCGGAATT-3'. All siRNAs were designed and synthesized by Guangzhou RiboBio Co., Ltd. (China).

Cell migration assay

To evaluate the role of *Bp*MOSPD2 and retromer components in LEAP2-mediated chemotaxis, *Bp*MO/MΦ cells were transfected with siRNAs targeting *BpMOSPD2*, *BpVPS35*, *BpVPS26*, or *BpVPS29*. Transwell assays were performed to assess *Bp*LEAP2-induced chemotaxis and *Bp*MOSPD2 and retromer component involvement. In all assays, 1 μg/mL scrambled peptide and 20% mudskipper serum were used as negative and positive controls, respectively. For the assay, *Bp*MO/MΦ cells transfected with scrambled or corresponding siRNAs were seeded in the upper Transwell chamber (2×10^5 cells/well) and 1 μg/mL *Bp*LEAP2 or control was added to the lower chamber. In a parallel setup, *Bp*MO/MΦ cells were pretreated with dimethyl sulfoxide (DMSO, #D4540, Sigma-Aldrich, USA) or 1 μg/mL brefeldin A (BFA; Sigma-Aldrich,

USA) for 30 min prior to exposure to *Bp*LEAP2 or control in the lower chamber. After incubation at 24°C with 5% CO_2 for 0, 4, 8, 12, or 24 h, cells on the lower surface of the upper chamber were gently washed twice with phosphate-buffered saline (PBS) and fixed with methanol for 20 min. Fixed cells were stained with 0.1% crystal violet (#V5265, Sigma-Aldrich, USA) for 30 min and washed three times with water. Non-migrated cells were gently removed with a cotton swab. Migrated cells were observed and imaged using a Nikon ECLIPSE Ni-E microscope (Japan). Five randomly selected fields (10×) from each sample were analyzed, with three biological replicates per treatment.

Mass spectrometry (MS) analysis

HEK293T cells were transfected with Flag-*BpMOSPD2*; empty vector transfected cells served as the negative control. At 48 h post-transfection, cells were lysed in buffer containing 20 mmol/L Tris-HCL (pH 8.0), 1% NP-40, 120 mmol/L NaCl, and 2 mmol/L EDTA, supplemented with protease (#32965, Thermo Fisher Scientific, USA) and phosphatase inhibitors (#P0001, Sigma-Aldrich, USA), and incubated at 4°C for 20 min. Lysates were centrifuged at 12 000 ×*g* for 10 min at 4°C, with the resulting supernatants incubated with anti-Flag agarose beads (#A2220, Sigma-Aldrich, USA) for 6 h at 4°C under constant agitation. Beads were washed four times with wash buffer (20 mmol/L Tris, pH 8.0; 100 mmol/L NaCl; 0.5 mmol/L EDTA, and 0.5% NP-40), then subjected to trypsin digestion at 37°C overnight. Digested peptides obtained from in-gel digestion were separated and analyzed using EASY-nLC 1000 ultra-performance liquid chromatography (UPLC) and tandem MS (LC-MS/MS) on a Q Exactive™ Plus mass spectrometer (Thermo Fisher Scientific, USA). The resulting data were processed using Proteome Discoverer v.2.4. The MS proteomic data were deposited in the ProteomeXchange Consortium via the PRIDE repository (PXD064369) (Deutsch et al., 2017).

Co-immunoprecipitation (Co-IP) and endogenous IP analysis

For the direct Co-IP assay, HEK293T cells were transfected with HA-*BpMOSPD2*, Flag-*BpVPS35*, or empty vector (Flag-Vector or HA-Vector). For the domain interaction Co-IP assay, HEK293T cells were transfected with HA-*BpMOSPD2*, HA-*BpMOSPD2ΔCRAL-TRIO* (HA-*BpMOSPD2ΔCT*), HA-*BpMOSPD2ΔMSP*, Flag-*BpVPS35*, or Flag-Vector. For the endogenous IP assay, HEK293T cells were transfected with Flag-*BpMOSPD2* or Flag-Vector, then treated with or without 1 μg/mL *Bp*LEAP2 for 12 h. Normal HEK293T cells served as a negative control. At 48 h post-transfection, cells were lysed in buffer containing protease and phosphatase inhibitors at 4°C for 20 min. The lysates were then centrifuged at 12 000 × *g* for 10 min at 4°C, with the resulting supernatants incubated with anti-Flag or anti-HA agarose (#A2095, Sigma-Aldrich, USA) beads for 6 h at 4°C. The beads were washed four times with wash buffer and subsequently subjected to western blot analysis.

Pull down assay

HEK293T cells were transfected with plasmids expressing HA-*BpMOSPD2*, Flag-*BpVPS26*, Flag-*BpVPS29*, or empty vector (Flag-Vector or HA-Vector). At 48 h post-transfection, cells were lysed with buffer containing protease and phosphatase inhibitors at 4°C for 20 min. The lysates were centrifuged at 12 000 ×*g* for 10 min at 4°C. The supernatants from individual transfections were combined and incubated together overnight at 4°C for proper interaction before pull down with anti-Flag or anti-HA agarose beads for 6 h at 4°C. Beads were washed four times with wash buffer and subsequently subjected to western blot analysis.

Cell fractionation

Cell fractionation was conducted using a Subcellular Protein Fractionation Kit for Cultured Cells (#78840, Thermo Fisher Scientific, USA) following the provided instructions. Briefly, HEK293T cells (1×10^6) were harvested and washed twice with ice-cold PBS, then lysed on ice in 200 μL of ice-cold cytoplasmic extraction buffer containing protease inhibitors for 10 min. Lysates were centrifuged at 500 ×*g* for 5 min, and the supernatant was collected as the cytoplasmic extract (CE). The remaining pellet was further lysed in 200 μL of membrane extraction buffer containing protease inhibitors for 10 min at 4°C, followed by centrifugation at 3 000 ×*g* for 5 min at 4°C to obtain the plasma membrane extract (ME) fraction.

Western blotting

Protein samples were prepared in 5×SDS loading buffer (250 mmol/L Tris-HCl (pH 6.8), 10% SDS, 5% β-mercaptoethanol, 50% glycerol, and 0.5% bromophenol blue) and boiled for 10 min. Equal amounts of protein were then subjected to sodium dodecyl sulfate-polyacrylamide gel electrophoresis (SDS-PAGE), followed by transfer to methanol-activated polyvinylidene fluoride (PVDF) membranes (#INCP00010, Millipore, USA). The membranes were then blocked in 5% non-fat milk for 1 h at room temperature and incubated overnight at 4°C with primary antibodies. After washing four times with TBST (20 mmol/L Tris, 100 mmol/L NaCl, and 0.1% Tween-20), membranes were incubated with appropriate secondary antibodies for 1 h at room temperature. Protein signals were developed using an ECL western blotting substrate (#32106, Thermo Fisher Scientific, USA; #WBKLS0500, Millipore, USA) and visualized using a western film processor. Band intensities were quantified using ImageJ.

Immunofluorescence

HeLa cells were seeded on glass slides at a density of 1×10^4 cells/slide and subjected to the following experimental conditions: (1) cotransfection with *BpMOSPD2* and *BpVPS35*, followed by treatment with or without 1 μg/mL *Bp*LEAP2 for 12 h; (2) cotransfection with *BpMOSPD2* and *BpVPS35*, followed by treatment with 1 μg/mL BFA for 30 min and subsequent stimulation with 1 μg/mL *Bp*LEAP2 for 12 h; and (3) siRNA-mediated knockdown of *hVPS35*, *hVPS26*, or *hVPS29*, followed by transfection with *BpMOSPD2* and treatment with 1 μg/mL *Bp*LEAP2 for 12 h. After treatment, cells were fixed with 4% paraformaldehyde (PFA) for 15 min, permeabilized with 0.5% saponin (#8047-15-2, Sigma-Aldrich, USA) for 15 min at room temperature, and washed three times with PBS. Blocking was performed using a buffer containing 1% bovine serum albumin (BSA, #A600332, BBI Life Sciences, China) and 22.52 mg/mL glycine in PBST. Cells were incubated with primary antibodies overnight at 4°C and then with corresponding immunofluorescence secondary antibodies for 1 h at room temperature. After additional PBS washes, the cells were mounted for imaging. Confocal imaging was performed using a Nikon AX-R confocal microscope (Japan) and image analysis was carried out using Nikon Elements Advanced Research v.6.02.01 (Japan). Manders' correlation coefficient was determined using the Coloc2 plugin in Fiji.

Antibodies

The following antibodies were used in this study: mouse anti-Flag (1:400 for immunofluorescence, #M20008, Abmart, China), rabbit anti-Flag (1:3 000 for western blot, #PA9001, Abmart, China), rabbit anti-HA (1:400 for immunofluorescence, 1:3 000 for western blot, #TT0050, Abmart, China), mouse anti-VPS35 (1:500 for western blot, #sc374372, Santa Cruz Biotechnology, USA), mouse anti-VPS26 (1:500 for western blot, #sc390304, Santa Cruz Biotechnology, USA), mouse anti-VPS29 (1:500 for western blot, #sc398874, Santa Cruz Biotechnology, USA), Alexa-Fluor-488-conjugated goat anti-rabbit (1:500, #A32731, Thermo Fisher Scientific, USA), Alexa-Fluor-555-conjugated goat anti-mouse (1:500, #A32727, Thermo Fisher Scientific, USA), horseradish peroxidase (HRP)-conjugated goat anti-rabbit IgG (1:3 000, #M21002, Abmart, China), and HRP-conjugated goat anti-mouse IgG (1:3 000 for western blot, #M21001, Abmart, China).

Reverse transcription-quantitative real-time polymerase chain reaction (RT-qPCR)

Total RNA was extracted using the RNAiso Plus Kit (#9109; Takara, Japan). cDNA was synthesized using HiScript III All-in-one RT SuperMix Perfect for RT-qPCR (#R333, Vazyme, China). RT-qPCR was conducted using Taq Pro Universal SYBR qPCR Master Mix (#Q712, Vazyme, China) on an ABI StepOne^{TM} Real-Time PCR System (Applied Biosystems, USA). Relative gene expression levels were calculated using the $2^{-\Delta\Delta CT}$ method, with *Bp18S rRNA* or *hGAPDH* as internal controls. Fold changes in gene expression at different time points were normalized to the control group. All primers utilized in RT-qPCR are provided in Supplementary Table S1.

Statistical analysis

Statistical analyses were performed using GraphPad Prism v.8 (USA). Differences between two groups were evaluated using Student's *t*-test. Data are presented as mean±standard deviation (SD). Each experiment was independently repeated at least three times, with statistical significance indicated as: ns: Not significant; *: $P<0.05$; **: $P<0.01$.

RESULTS

*Bp*LEAP2 stimulation promotes *Bp*MOSPD2 membrane trafficking to mediate *Bp*MO/MΦ chemotaxis

Our previous studies identified *Bp*LEAP2 as an immunomodulatory peptide that promotes *Bp*MO/MΦ chemotaxis, with *Bp*MOSPD2 functioning as its putative receptor (Chen et al., 2016; Li et al., 2020). To elucidate how *Bp*MOSPD2—which is predominantly localized to intracellular compartments under basal conditions (Di Mattia et al., 2018)—participates in plasma membrane-associated signaling, the subcellular trafficking dynamics of *Bp*MOSPD2 in response to *Bp*LEAP2 stimulation were examined.

Treatment with 1 μg/mL *Bp*LEAP2, but not the scrambled control peptide, induced a robust and time-dependent increase in *Bp*MO/MΦ migration, peaking at 12 h post-stimulation and declining by 24 h (Figure 1A, B). Mudskipper serum, used as a positive control due to its endogenous cytokine and chemokine content, elicited a similarly time-dependent chemotactic response. Silencing of *BpMOSPD2* via siRNA significantly attenuated *Bp*LEAP2-induced migration, despite continuous *Bp*LEAP2 exposure, thereby confirming its essential role in mediating this effect (Figure 1A, B; Supplementary Figure S1A).

To determine how an intracellularly localized receptor mediates extracellular ligand sensing, *Bp*MOSPD2 membrane trafficking was investigated following *Bp*LEAP2 stimulation. Subcellular fractionation revealed a marked increase in the membrane-associated fraction of *Bp*MOSPD2 after 12 h of stimulation (Figure 1C). Immunofluorescence analysis showed enhanced colocalization of *Bp*MOSPD2 with the early endosome marker EEA1, along with decreased overlap with the ER marker calnexin (Di Mattia et al., 2018). Localization to the trans-Golgi network (TGN38) and lysosomes (Lamp1) remained largely unchanged (Figure 1D–H).

These findings suggest that *Bp*LEAP2 may drive the relocalization of *Bp*MOSPD2 from the ER to early endosomes and subsequently to the plasma membrane. This endosome-mediated trafficking pathway likely enables *Bp*MOSPD2 to reposition to the cell surface, where it functions as a receptor for *Bp*LEAP2 and initiates downstream signaling events that promote *Bp*MO/MΦ chemotaxis.

Retromer complex governs retrograde trafficking of *Bp*MOSPD2 from early endosomes to the plasma membrane

To determine whether post-ER trafficking is required for *Bp*MOSPD2 surface delivery, ER export was blocked with BFA (1 μg/mL, 30 min pre-treatment), followed by *Bp*MO/MΦ stimulation. Confocal imaging coupled with organelle markers revealed a pronounced redistribution of *Bp*MOSPD2: colocalization with the early endosome marker EEA1 decreased by 16% (Manders' coefficient, $P<0.05$), while overlap with the ER marker calnexin increased by 12% (Figure 2A–E). In contrast, no significant changes were observed in association with trans-Golgi (TGN38) or lysosomal (Lamp1) markers (Figure 2A–E), suggesting that *Bp*MOSPD2 exits the ER through a BFA-sensitive pathway specifically directed toward early endosomes. Consistently, subcellular fractionation confirmed that BFA treatment reduced the plasma membrane-associated fraction of *Bp*MOSPD2 by 65%, with no change in the cytoplasmic fraction (Figure 2F), consistent with impaired ER-to-membrane trafficking.

Because canonical ER-Golgi trafficking does not fully account for receptor recycling from endosomes to the plasma membrane (Naslavsky & Caplan, 2018), MS analysis was employed to identify trafficking regulators interacting with *Bp*MOSPD2. Flag-tagged *Bp*MOSPD2 immunoprecipitates from HEK293T cells were analyzed by LC-MS/MS. Notably, all three core components of the retromer complex—VPS35, VPS26, and VPS29—were among the prominent trafficking-related interactors, each represented by multiple high-confidence peptides (Figure 2G–J). Endogenous co-immunoprecipitation confirmed these interactions: *Bp*MOSPD2 robustly pulled down VPS35, VPS26, and VPS29, with binding significantly enhanced following 12 h of *Bp*LEAP2 stimulation (Figure 2K). Given that the retromer complex mediates cargo sorting on endosomes and facilitates retrograde transport to either the trans-Golgi network or plasma membrane, thereby preventing lysosomal degradation, these findings suggest that the retromer complex is a critical trafficking partner of *Bp*MOSPD2 and that retromer-mediated retrograde transport is indispensable for delivering *Bp*MOSPD2 from early endosomes to the plasma membrane.

*Bp*MOSPD2 physically interacts with *Bp*VPS35 independent of its MSP and CRAL-TRIO domains

To define the molecular interface between *Bp*MOSPD2 and the retromer complex, analysis focused on *Bp*VPS35, the central

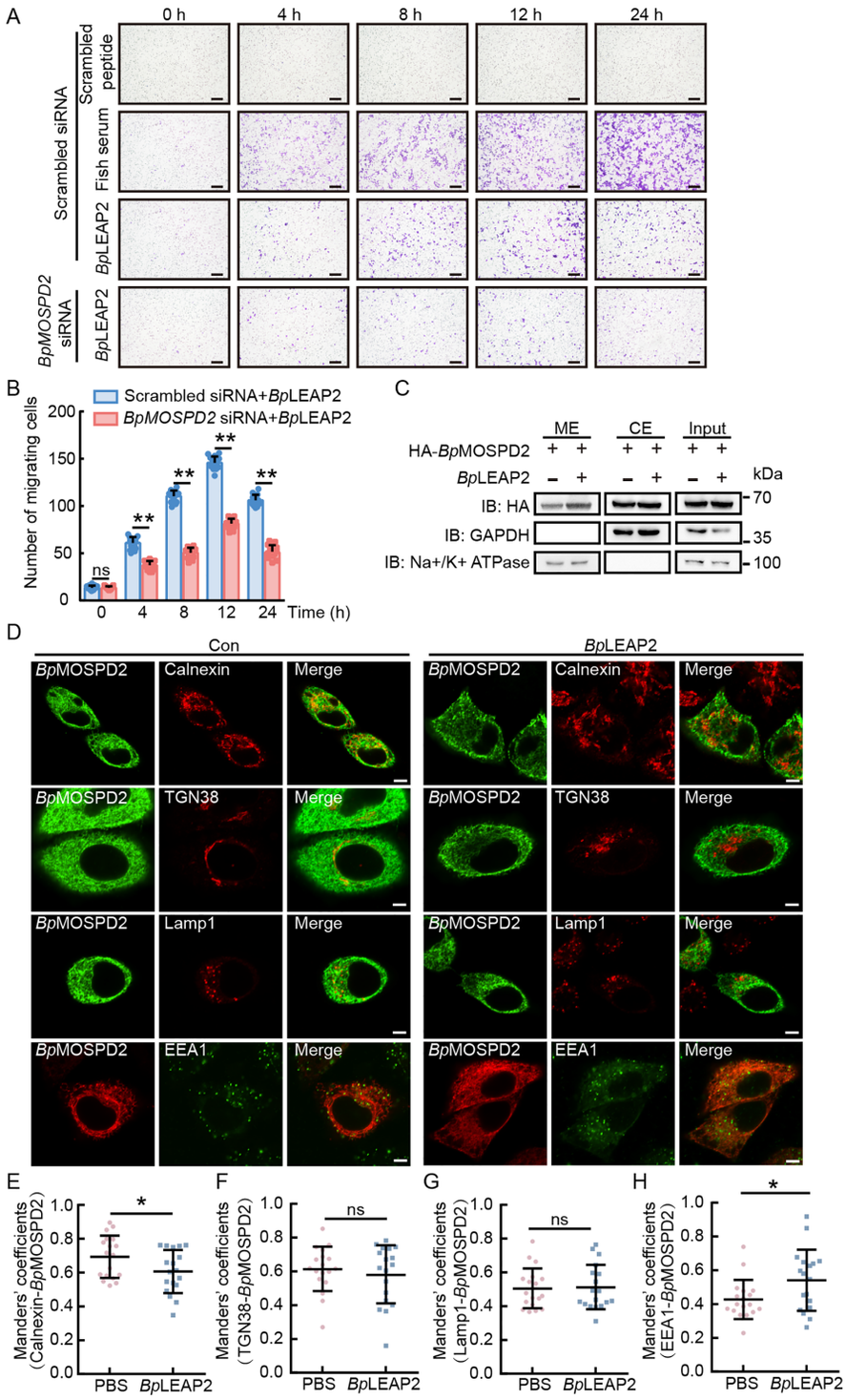

Figure 1 *Bp*LEAP2 stimulation promotes *Bp*MOSPD2 membrane localization and enhances *Bp*MO/MΦ chemotaxis

A: Transwell migration assays of *Bp*MO/MΦ cells transfected with either scrambled or *BpMOSPD2* siRNAs and seeded in the upper chamber, with 1 μg/mL *Bp*LEAP2 added to the lower chamber. Scrambled peptide (1 μg/mL) and 20% fish (mudskipper) serum were included as negative and positive controls, respectively. Chemotaxis was assessed after 0, 4, 8, 12, or 24 h of incubation. Migrated cells were stained with crystal violet and visualized at 10× magnification. Scale bars: 100 μm. B: Quantification of *Bp*LEAP2-induced migrating cells shown in A. Each time point includes three biological replicates, with five random fields counted per well. C: Immunoblot analysis of plasma membrane extract (ME) and cytoplasmic extract (CE) fractions from HEK293T cells overexpressing HA-*Bp*MOSPD2, with or without 1 μg/mL *Bp*LEAP2 treatment for 12 h. Na^+/K^+ ATPase and GAPDH were used as markers for ME and CE fractions, respectively. D: Immunofluorescence staining of HeLa cells expressing Flag-*Bp*MOSPD2 and treated with 1 μg/mL *Bp*LEAP2 for 12 h. HeLa cells were labeled with four organelle marker antibodies (endoplasmic reticulum (ER): calnexin; trans Golgi apparatus: TGN38; late endosome/lysosome: Lamp1; early endosome: EEA1) and anti-Flag antibodies. Scale bars: 5 μm. E–H: Manders' overlap coefficients quantifying the colocalization of *Bp*MOSPD2 with calnexin (E), TGN38 (F), Lamp1 (G), and EEA1 (H) under PBS or 1 μg/mL *Bp*LEAP2 treatment. Each dot represents a single cell (n=18 cells from three independent experiments). Statistical significance was assessed using unpaired two-tailed Student's t-test. Data are presented as mean±SD. ns: Not significant; *: P<0.05; **: P<0.01.

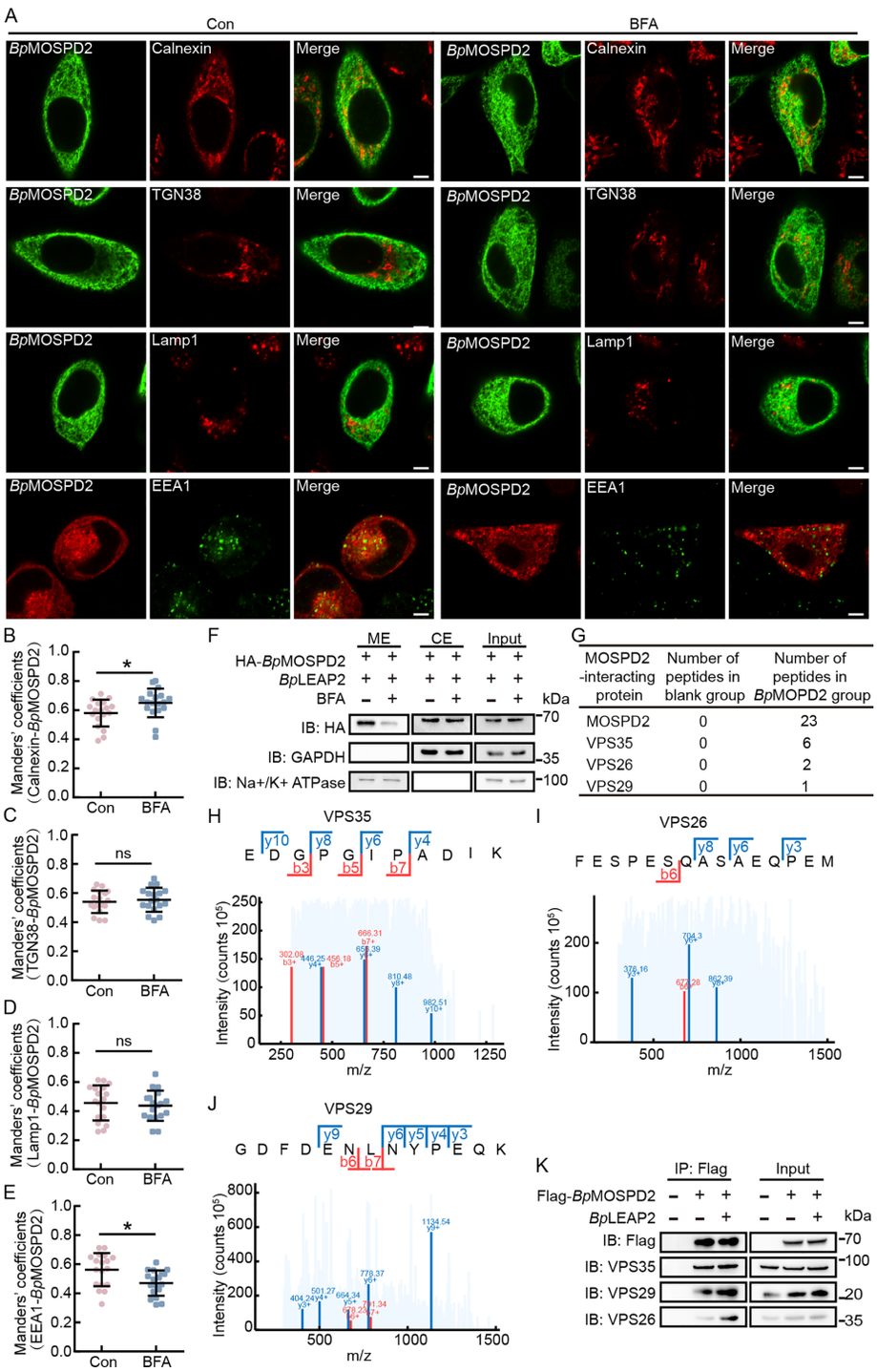

Figure 2 Identification of the retromer complex as a *Bp*MOSPD2 interactor

A: Immunofluorescence staining of HeLa cells expressing Flag-*Bp*MOSPD2, pretreated with 1 μg/mL brefeldin A (BFA) or DMSO for 30 min, followed by 1 μg/mL *Bp*LEAP2 for 12 h. Cells were colabeled with anti-Flag antibodies and markers for the four organelles. ER: Calnexin; trans Golgi apparatus: TGN38; late endosome/lysosome: Lamp1; early endosome: EEA1. Scale bars: 5 μm. B–E: Quantification of *Bp*MOSPD2 colocalization with calnexin (B), TGN38 (C), Lamp1 (D), and EEA1 (E) using Manders' overlap coefficients. Each dot represents a single cell (n=18 cells from three independent experiments). F: Immunoblot analysis of ME and CE fractions from HEK293T cells overexpressing HA-*Bp*MOSPD2, with or without BFA treatment under 1 μg/mL *Bp*LEAP2 for 12 h. Na^+/K^+-ATPase and GAPDH served as markers for plasma membrane and cytoplasmic fractions, respectively. G: Mass spectrometry (MS) analysis of proteins co-immunoprecipitated with Flag-*Bp*MOSPD2 identified core retromer complex subunits. Flag-*Bp*MOSPD2 was pulled down from transfected HEK293T lysates using anti-Flag agarose beads under stringent washing conditions. H–J: Representative MS spectra for peptides derived from VPS35 (H), VPS26 (I), and VPS29 (J) detected in *Bp*MOSPD2 pulldown samples. K: Co-immunoprecipitation (Co-IP) of endogenous VPS35, VPS26, and VPS29 with Flag-*Bp*MOSPD2 in HEK293T cells treated or untreated with 1 μg/mL *Bp*LEAP2 for 12 h, confirming interaction observed by MS. Flag-Vector denotes an empty vector carrying the Flag tag, transfected in place of the target gene construct, serving as a negative control. Statistical significance was assessed using unpaired two-tailed Student's t-test. Data are presented as mean±SD. ns: Not significant; *: P<0.05; **: P<0.01.

cargo-recognition subunit (Kovtun et al., 2018). Co-expression of Flag-tagged *BpVPS35* and *BpMOSPD2* in HEK293T cells followed by reciprocal Co-IP confirmed robust and specific physical interaction, irrespective of which protein was used as bait (Figure 3A). In contrast, pull-down assays revealed no detectable association between *Bp*MOSPD2 and either *Bp*VPS26 or *Bp*VPS29, identifying *Bp*VPS35 as the sole retromer component engaging with *Bp*MOSPD2 (Figure 3B, C). *Bp*MOSPD2 contains two conserved cytoplasmic domains: an MSP domain and a CRAL-TRIO (CT) domain. To evaluate whether either domain is required for *Bp*VPS35 binding, deletion mutants lacking the MSP domain (ΔMSP) or CRAL-TRIO domain (ΔCT) were constructed. Of note, Co-IP revealed that both deletion variants retained the ability to associate with *Bp*VPS35 at levels comparable to full-length *Bp*MOSPD2 (Figure 3B), indicating that neither domain is essential for retromer engagement. These findings suggest that *Bp*MOSPD2 engages *Bp*VPS35 through alternative regions or via an indirect mechanism involving additional scaffolding factors.

To further validate this interaction and assess its dynamic regulation by *Bp*LEAP2, immunofluorescence colocalization analysis was performed in HeLa cells co-expressing *Bp*MOSPD2 and *Bp*VPS35. Under basal conditions, moderate spatial overlap was observed. Following 12 h of stimulation with 1 μg/mL *Bp*LEAP2, colocalization was significantly enhanced, as quantified by Manders' overlap coefficient (Figure 3D, F), indicating that *Bp*LEAP2 promotes or stabilizes the *Bp*MOSPD2-retromer interaction. Collectively, these results identify *Bp*VPS35 as a direct trafficking partner of *Bp*MOSPD2 and implicate their association as a regulated node in the *Bp*LEAP2-induced chemotactic pathway.

Functional integrity of the retromer complex is essential for *Bp*MOSPD2 plasma membrane targeting

Given the physical association between *Bp*MOSPD2 and *Bp*VPS35, we hypothesized that a fully assembled retromer complex is necessary for proper membrane trafficking of *Bp*MOSPD2. To test this, HEK293T cells were transfected with siRNA-mediated silencing of *VPS35*, *VPS26*, or *VPS29* prior

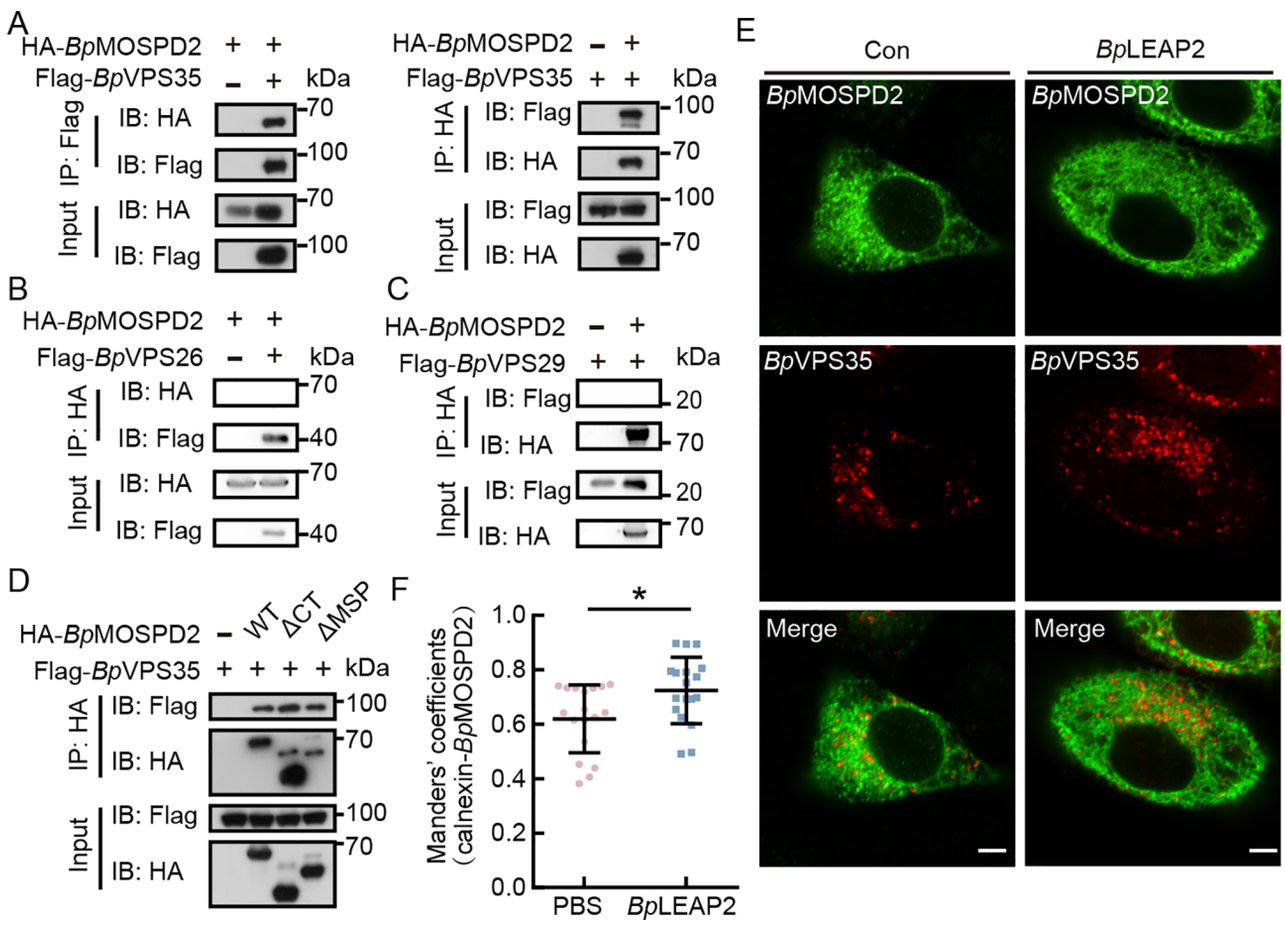

Figure 3 Identification of *Bp*VPS35 as a *Bp*MOSPD2 interactor

A: Co-IP assays were performed in HEK293T cells cotransfected with HA-tagged Bp*MOSPD2*, Flag-tagged *BpVPS35*, or empty vector (Flag-Vector or HA-Vector) for 48 h. Cell lysates were incubated with anti-Flag or anti-HA agarose beads for 6 h, washed extensively, and subjected to immunoblotting with anti-Flag and anti-HA antibodies. B, C: Pull down assays to confirm direct interactions between HA-*Bp*MOSPD2 and either Flag-*Bp*VPS26 (B) or Flag-*Bp*VPS29 (C). D: Co-IP assays using HA-tagged *Bp*MOSPD2 deletion mutants were conducted to assess the role of the MSP and CRAL-TRIO (CT) domains in mediating interaction with Flag-BpVPS35. Flag-Vector represents an empty vector carrying the Flag tag, transfected in place of the target gene construct, serving as a negative control. E: Immunofluorescence staining of HeLa cells co-expressing Flag-*BpMOSPD2* and HA-*BpVPS35* following PBS or 1 μg/mL *Bp*LEAP2 treatment for 12 h. Cells were stained with anti-Flag (green) and anti-HA (red) antibodies. Scale bars: 5 μm. F: Quantification of *Bp*MOSPD2 and *Bp*VPS35 colocalization using Manders' overlap coefficients under control (PBS) or 1 μg/mL *Bp*LEAP2 stimulation. Each dot represents a single cell (n=18 cells from three independent experiments). Statistical significance was assessed using unpaired two-tailed Student's t-test. Data are presented as mean±SD. ns: Not significant; *: P<0.05; **: P<0.01.

to *Bp*MOSPD2 overexpression and *Bp*LEAP2 stimulation. Knockdown efficiency for each subunit was confirmed by RT-qPCR (Supplementary Figure S1B–D). Subcellular fractionation revealed that depletion of any single retromer component resulted in a marked reduction of *Bp*MOSPD2 in the membrane fraction, with densitometric quantification indicating reductions of 35%–46% relative to scrambled siRNA controls (Figure 4A, B). These results indicate that the entire retromer core complex is required for efficient membrane recruitment.

To determine whether this trafficking defect reflects impaired endosomal trafficking, immunofluorescence analysis was performed in HeLa cells following siRNA-mediated knockdown of *VPS35*, *VPS26*, or *VPS29* (Supplementary Figure S1E–G). In control siRNA-transfected HeLa cells, *Bp*MOSPD2 exhibited partial colocalization with the early endosome marker EEA1 following *Bp*LEAP2 stimulation, consistent with its transient passage through this compartment. However, knockdown of any of the three retromer subunits significantly enhanced this colocalization (Figure 4C–J), suggesting that *Bp*MOSPD2 accumulates within early endosomes when retromer-mediated export is impaired. In contrast, localization relative to the ER (calnexin), trans-Golgi network (TGN38), and lysosomes (Lamp1) remained largely unchanged (Figure 4C–J).

Together, these findings demonstrate that functional retromer activity is essential for the trafficking of *Bp*MOSPD2 from early endosomes to the plasma membrane, a prerequisite for its functional positioning and engagement in *Bp*LEAP2-driven signaling.

Retromer complex is required for *Bp*LEAP2-*Bp*MOSPD2-mediated *Bp*MO/MΦ chemotaxis

Having established that *Bp*MOSPD2 relies on the retromer complex for endosomal exit and plasma membrane localization, the functional relevance of this trafficking machinery in *Bp*LEAP2-induced *Bp*MO/MΦ migration was next evaluated. As expected, inhibition of ER export with 1 μg/mL BFA significantly suppressed *Bp*LEAP2-induced chemotaxis at all measured time points, with maximal inhibition observed at 12 h post-treatment (Figure 5A, B).

To determine the specific requirement for retromer activity, *Bp*MO/MΦ cells were subjected to siRNA-mediated knockdown of *BpVPS35*, *BpVPS26*, or *BpVPS29* (Supplementary Figure S1H–J). Remarkably, silencing of any individual subunit led to a pronounced and sustained reduction in *Bp*LEAP2-triggered chemotaxis (Figure 5C, D). The magnitude of suppression closely resembled that observed upon *BpMOSPD2* knockdown, suggesting functional convergence within the same signaling axis.

Collectively, these findings demonstrate that retromer-mediated trafficking is required for *Bp*MOSPD2 surface localization and for the propagation of *Bp*LEAP2-mediated chemotactic signals. The retromer complex thus acts as a critical regulator of peptide-directed MO/MΦ migration in this teleost model.

DISCUSSION

In teleosts, MO/MΦ serve as pivotal effectors of the innate immune system, executing core functions, including phagocytosis, cytokine production, and antimicrobial defense, paralleling roles observed in mammals. Extensive evidence supports that chemokine-induced cytoskeletal remodeling and innate immune activation contribute to the conserved effector functions of MO/MΦ across vertebrates, emphasizing their central role in host defense (Grayfer et al., 2018; Zhang et al., 2024). In teleosts, where adaptive immunity is comparatively limited, mononuclear phagocytes exhibit innate responsiveness and broad immunological reactivity. Their rapid chemotactic responses to immunomodulatory cues such as LEAP2 reflect a finely tuned migratory capacity that demands precise regulation. Elucidating the upstream mechanisms governing receptor trafficking and intracellular signaling is essential for understanding how spatial and temporal immune control is achieved in lower vertebrate lineages.

LEAP2, originally characterized as a teleost-specific, hepatically enriched antimicrobial peptide, functions as a potent immunomodulatory cue in *B. pectinirostris*, with previous studies implicating *Bp*MOSPD2 as its functional receptor (Chen et al., 2016; Li et al., 2020). Although classically defined as a plasma membrane protein in mammalian monocytes and cancer cells, emerging evidence has expanded the subcellular localization of MOSPD2 to include ER compartments and interorganelle contact sites, suggesting a broader functional repertoire (Di Mattia et al., 2018; Mendel et al., 2017; Salem et al., 2019; Zouiouich et al., 2022). The present study expands the functional landscape of MOSPD2 in teleosts, identifying *Bp*MOSPD2 as a dynamically trafficked, stimulus-inducible chemotactic receptor whose mobilization relies on retromer-dependent sorting from endosomal compartments to the cell surface.

Stimulation with recombinant *Bp*LEAP2 elicited robust chemotactic responses in primary *Bp*MO/MΦ cultures, a process abrogated by targeted knockdown of *Bp*MOSPD2 (Figure 1A, B). In parallel, subcellular fractionation and immunofluorescence analyses demonstrated that *Bp*LEAP2 engagement induced a pronounced redistribution of *Bp*MOSPD2 from the endoplasmic reticulum to early endosomes, followed by accumulation at the plasma membrane. This polarized trafficking pattern was not accompanied by relocalization to the trans-Golgi network or lysosomal compartments, indicating selective endosomal routing. These results collectively indicate that LEAP2 promotes spatial reprogramming of *Bp*MOSPD2 toward membrane-localized signaling platforms, where it transduces directional migration cues with temporal precision.

This trafficking trajectory was further substantiated through both pharmacological and genetic approaches. Disruption of ER export with BFA resulted in marked depletion of early endosomal *Bp*MOSPD2 and a pronounced reduction in its membrane-associated pool, indicating that ER-to-endosome transit is a prerequisite for surface redistribution (Figure 2A, E, F). To elucidate the trafficking machinery underlying *Bp*MOSPD2 mobilization, immunoprecipitation coupled with MS was conducted, revealing VPS35, VPS26, and VPS29—core components of the retromer complex—as interacting partners (Figure 2G–J). Endogenous co-immunoprecipitation corroborated these interactions and demonstrated their up-regulation following *Bp*LEAP2 stimulation (Figure 2K), indicating the inducible formation of a *Bp*MOSPD2-retromer complex in response to external cues.

The retromer complex constitutes an evolutionarily conserved trafficking hub that orchestrates the selective recycling of transmembrane proteins to the plasma membrane or trans-Golgi network, thereby protecting them from lysosomal degradation (Bingham et al., 2024; Trousdale & Kim, 2015; Vagnozzi & Praticò, 2019). Established cargos include β2-adrenergic receptors (β2ARs), mannose 6-phosphate receptor

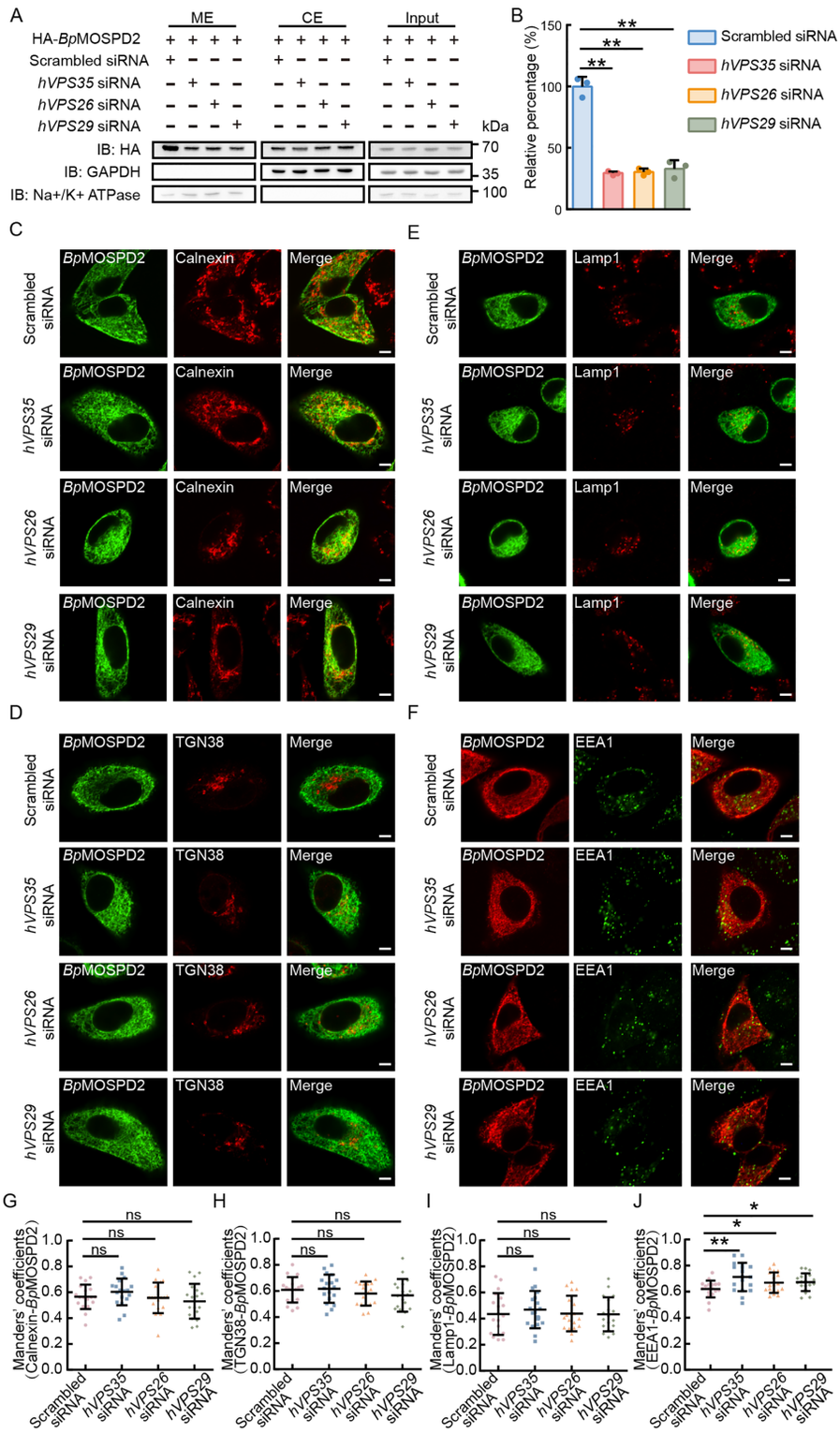

Figure 4 Retromer complex is required for *Bp*MOSPD2 membrane trafficking

A: Western blot analysis of membrane (ME) and cytoplasmic extract (CE) fractions from HEK293T cells transfected with HA-tagged *BpMOSPD2* and siRNAs targeting *VPS35*, *VPS26*, or *VPS29*, followed by stimulation with 1 μg/mL *Bp*LEAP2 for 12 h. Na^+/K^+-ATPase and GAPDH served as markers for ME and CE fractions, respectively. B: Densitometric quantification of *Bp*MOSPD2 abundance in the membrane fraction, normalized to Na^+/K^+-ATPase. Values are expressed as percentages relative to the scrambled siRNA control, which was set to 100% (n=3 biological replicates). C–F: Immunofluorescence staining of HeLa cells cotransfected with *Bp*MOSPD2 and siRNA targeting *VPS35*, *VPS26*, or *VPS29*, followed by 1 μg/mL *Bp*LEAP2 treatment for 12 h. Cells were labeled with antibodies against *BpMOSPD2* and organelle-specific markers: calnexin (C); TGN38 (D); Lamp1 (E), and EEA1 (F). G–J: Quantification of *Bp*MOSPD2 colocalization with calnexin (G), TGN38 (H), Lamp1 (I), and EEA1 (J) using Manders' overlap coefficients under indicated knockdown conditions. Each dot represents a single cell (n=18 cells from three independent experiments). Statistical significance was assessed using unpaired two-tailed Student's t-test. Data are presented as mean±SD. ns: Not significant; *: P<0.05; **: P<0.01.

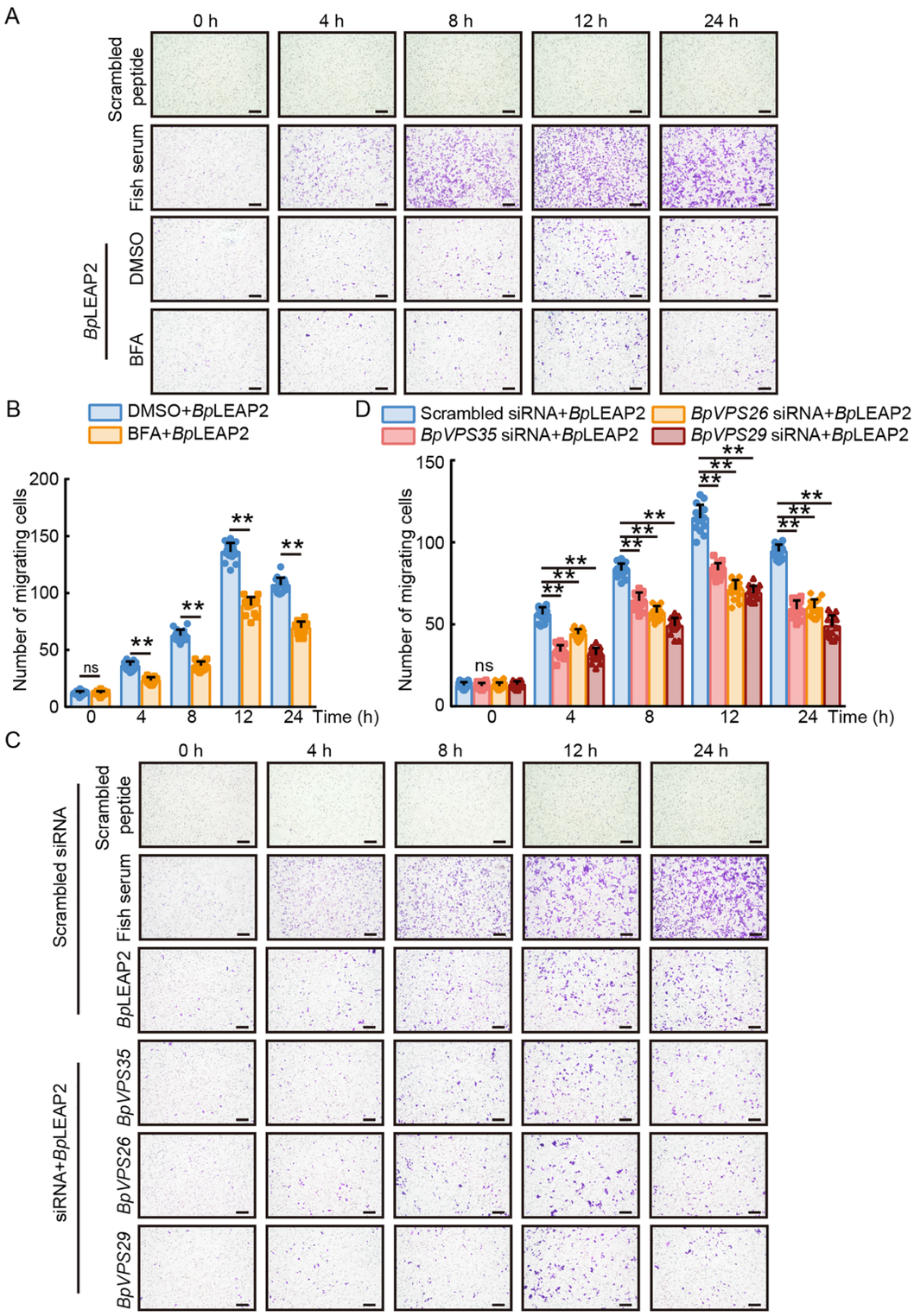

Figure 5 Retromer complex is required for *Bp*LEAP2-induced chemotaxis of *Bp*MO/MΦ cells

A: Transwell migration assay of *Bp*MO/MΦ cells seeded in the upper chamber, with 1 μg/mL *Bp*LEAP2 applied to the lower chamber in the presence of DMSO or 1 μg/mL BFA. Scrambled peptide (1 μg/mL) and 20% mudskipper serum served as negative and positive controls, respectively. Chemotactic responses were assessed at 0, 4, 8, 12, or 24 h. Migrated cells were stained with crystal violet and imaged under a microscope at 10× magnification. Scale bars: 100 μm. B: Quantification of *Bp*LEAP2-induced migrated cells in A. Each time point includes three biological replicates, with five random fields counted per well. C: Transwell migration assay of *Bp*MO/MΦ cells transfected with scrambled siRNA or siRNAs targeting *BpVPS35*, *BpVPS26*, or *BpVPS29*. Cells were seeded in the upper chamber, and 1 μg/mL *Bp*LEAP2 was added to the lower chamber. Chemotaxis was assessed at 0, 4, 8, 12, or 24 h. Migrated cells were stained with crystal violet and imaged at 10× magnification. Scale bars: 100 μm. D: Quantification of *Bp*LEAP2-induced migration from C. Each time point includes three biological replicates, with five random fields counted per well. Statistical significance was assessed using unpaired two-tailed Student's *t*-test. Data are presented as mean±SD. ns: Not significant; *: $P<0.05$; **: $P<0.01$.

(CI-MPR), β-secretase 1, and triggering receptor expressed on myeloid cells 2 (Trem2) (Choy et al., 2014; Seaman, 2004; Wen et al., 2011; Yu et al., 2023). The present findings establish *Bp*MOSPD2 as a previously unrecognized retromer cargo in a teleost innate immune context. Notably, interactions between *Bp*MOSPD2 and *Bp*VPS35 persisted despite deletion of either the MSP or CRAL-TRIO domain (Figure 3A, B), suggesting that the retromer binding interface lies elsewhere within the protein or based on its scaffolding structures.

Targeted disruption of retromer complex function through siRNA-mediated silencing of *VPS35*, *VPS26*, or *VPS29* markedly reduced *Bp*MOSPD2 plasma membrane localization and resulted in its retention within early endosomes (Figure 4A, B, F, J). This intracellular retention was not accompanied by compensatory redistribution to the ER, trans-Golgi network, or lysosomal compartments, indicating a selective impairment in endosome-to-membrane trafficking. These findings identify the retromer complex as an essential mediator of *Bp*MOSPD2 recycling, required for its functional relocalization to the plasma membrane.

The physiological consequence of this trafficking defect is profound: retromer deficiency, whether by VPS35, VPS26, or VPS29 depletion, significantly impairs *Bp*LEAP2-induced *Bp*MO/MΦ migration, phenocopying the effects of *BpMOSPD2* knockdown or ER export blockade (Figure 5). These data place retromer-dependent trafficking as a central regulatory node in the *Bp*LEAP2-*Bp*MOSPD2 signaling axis. This mechanism mirrors established paradigms in mammalian systems where retromer integrity is required for receptor recycling and signaling fidelity, yet our findings extend this model into the realm of innate peptide sensing in lower vertebrates.

This study reveals a previously uncharacterized trafficking mechanism in which *Bp*LEAP2 stimulation triggers the retromer-dependent redistribution of *Bp*MOSPD2 from intracellular compartments to the plasma membrane, a spatial repositioning event required for eliciting directed migration in *Bp*MO/MΦ. These findings not only establish *Bp*MOSPD2 as a functional receptor for *Bp*LEAP2 in mediating the biological activities of *Bp*MO/MΦ cells but also reveal that the retromer complex mediates the retrograde transport of *Bp*MOSPD2 (Figure 6). Previous studies have demonstrated that MOSPD2 mediates CCL5-induced chemotaxis in human monocytes via activation

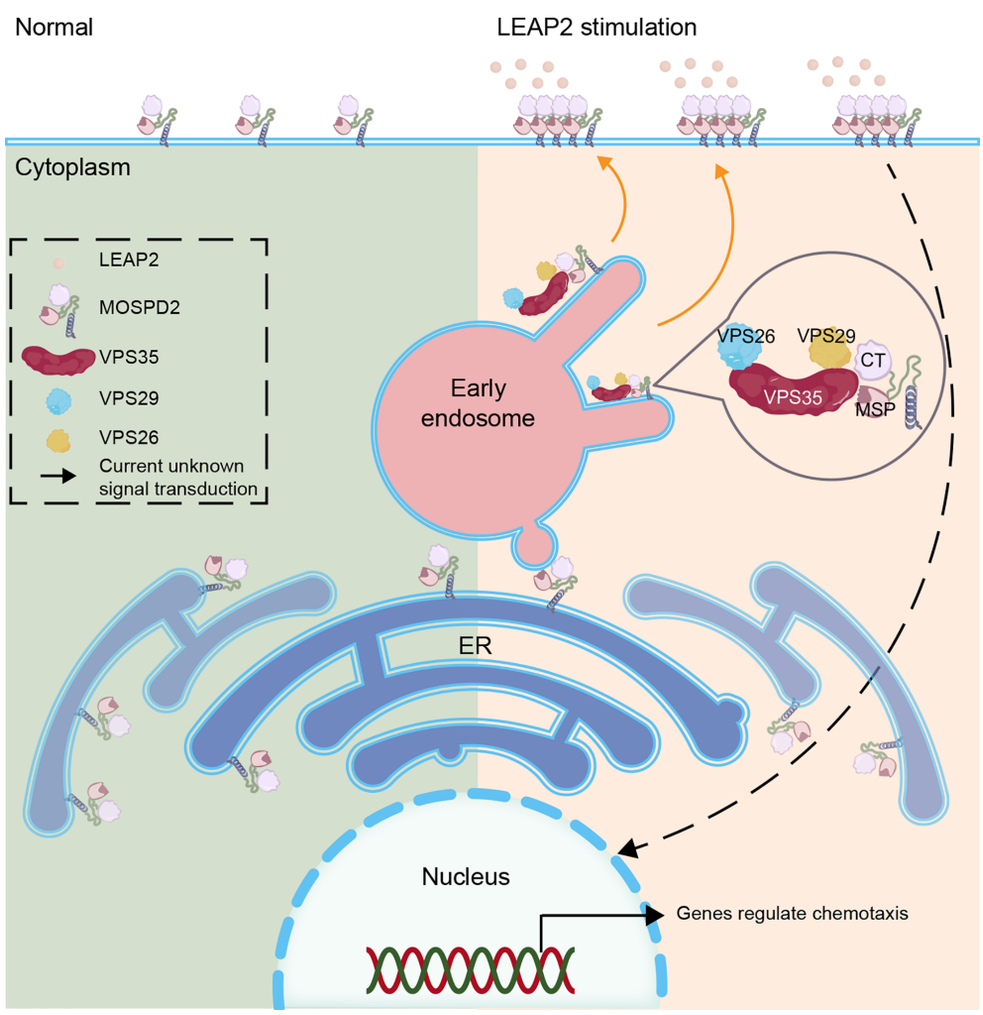

Figure 6 Schematic model of LEAP2-induced retromer-dependent trafficking and chemotactic signaling of MOSPD2

Under basal conditions (left panel), *Bp*MOSPD2 is predominantly localized to the endoplasmic reticulum (ER), with minimal presence at the plasma membrane. Upon *Bp*LEAP2 stimulation (right panel), *Bp*MOSPD2 translocates to early endosomes, where it associates with the core retromer complex—comprising VPS35, VPS29, and VPS26. This interaction facilitates the recycling of *Bp*MOSPD2 to the plasma membrane. Surface accumulation of *Bp*MOSPD2 and engagement with *Bp*LEAP2 are proposed to initiate as yet undefined intracellular signaling cascades, ultimately promoting the transcriptional activation of genes involved in MO/MΦ chemotaxis. This model illustrates the dynamic redistribution of *Bp*MOSPD2 and its retromer-mediated trafficking pathway in response to *Bp*LEAP2.

of the ERK1/2 and AKT signaling pathways (Mendel et al., 2017) and promotes breast cancer cell migration through EGFR engagement and downstream signaling via the same cascades (Salem et al., 2019). Although the intracellular pathways linking MOSPD2 to LEAP2-triggered motility remain undefined in teleost immune cells, these findings provide a mechanistic precedent suggesting that *Bp*LEAP2-*Bp*MOSPD2 signaling may likewise engage conserved pathways such as AKT or ERK to promote chemotactic responses. Future studies are required to determine whether these or other signaling mechanisms are activated upon *Bp*MOSPD2 accumulation at the plasma membrane in response to *Bp*LEAP2 stimulation.

SUPPLEMENTARY DATA

Supplementary data to this article can be found online.

COMPETING INTERESTS

The authors declare that they have no competing interests.

AUTHORS' CONTRIBUTIONS

Conceptualization: T.F.Z., L.N., J.Z.S., and J.C.; Methodology: T.F.Z. and L.N.; Investigation: T.F.Z., Z.Y.Z., C.J.F., and S.C.S.; Visualization: T.F.Z.; Funding acquisition: J.C.; Project administration: L.N., J.Z.S., and J.C.; Supervision: L.N., J.Z.S., and J.C.; Writing – original draft: T.F.Z.; Writing – review & editing: T.F.Z., L.N., J.Z.S., and J.C. All authors read and approved the final version of the manuscript.

REFERENCES

Bingham R, McCarthy H, Buckley N. 2024. Exploring retrograde trafficking: mechanisms and consequences in cancer and disease. *Traffic*, **25**(2): e12931.

Chen J, Chen Q, Lu XJ, et al. 2016. The protection effect of LEAP-2 on the mudskipper (*Boleophthalmus pectinirostris*) against *Edwardsiella tarda* infection is associated with its immunomodulatory activity on monocytes/macrophages. *Fish & Shellfish Immunology*, **59**: 66–76.

Choy RWY, Park M, Temkin P, et al. 2014. Retromer mediates a discrete route of local membrane delivery to dendrites. *Neuron*, **82**(1): 55–62.

Deutsch EW, Csordas A, Sun Z, et al. 2017. The ProteomeXchange consortium in 2017: supporting the cultural change in proteomics public data deposition. *Nucleic Acids Research*, **45**(D1): D1100–D1106.

Di Mattia T, Wilhelm LP, Ikhlef S, et al. 2018. Identification of MOSPD2, a novel scaffold for endoplasmic reticulum membrane contact sites. *EMBO Reports*, **19**(7): e45453.

Edgar AJ, Polak JM. 2000. Human homologues of yeast vacuolar protein sorting 29 and 35. *Biochemical and Biophysical Research Communications*, **277**(3): 622–630.

Grayfer L, Kerimoglu B, Yaparla A, et al. 2018. Mechanisms of fish macrophage antimicrobial immunity. *Frontiers in Immunology*, **9**: 1105.

Haft CR, De La Luz Sierra M, Bafford R, et al. 2000. Human orthologs of yeast vacuolar protein sorting proteins VPS26, 29, and 35: assembly into multimeric complexes. *Molecular Biology of the Cell*, **11**(12): 4105–4116.

James C, Kehlenbach RH. 2021. The interactome of the VAP family of proteins: an overview. *Cells*, **10**(7): 1780.

Kovtun O, Leneva N, Bykov YS, et al. 2018. Structure of the membrane-assembled retromer coat determined by cryo-electron tomography. *Nature*, **561**(7724): 561–564.

Li CH, Chen J, Nie L, et al. 2020. MOSPD2 is a receptor mediating the LEAP-2 effect on monocytes/macrophages in a teleost, *Boleophthalmus pectinirostris*. *Zoological Research*, **41**(6): 644–655.

Mendel I, Yacov N, Salem Y, et al. 2017. Identification of motile sperm domain-containing protein 2 as regulator of human monocyte migration. *The Journal of Immunology*, **198**(5): 2125–2132.

Naslavsky N, Caplan S. 2018. The enigmatic endosome - sorting the ins and outs of endocytic trafficking. *Journal of Cell Science*, **131**(13): jcs216499.

Neefjes J, Cabukusta B. 2021. What the VAP: The expanded VAP family of proteins interacting with FFAT and FFAT-related motifs for interorganellar contact. *Contact (Thousand Oaks)*, **4**: 25152564211012246.

Nie L, Wu XY, Zhao ZY, et al. 2025. Palmitoylation-mediated NLRP3 inflammasome activation in teleosts highlights evolutionary divergence in immune regulation. *Zoological Research*, **46**(1): 3–14.

Salem Y, Yacov N, Kafri P, et al. 2025. MOSPD2 regulates the activation state of αLβ2 integrin to control monocyte migration: applicability for treatment of chronic inflammatory diseases. *Immunologic Research*, **73**(1): 78.

Salem Y, Yacov N, Propheta-Meiran O, et al. 2019. Newly characterized motile sperm domain-containing protein 2 promotes human breast cancer metastasis. *International Journal of Cancer*, **144**(1): 125–135.

Seaman MNJ. 2004. Cargo-selective endosomal sorting for retrieval to the Golgi requires retromer. *Journal of Cell Biology*, **165**(1): 111–122.

Seaman MNJ. 2021. The retromer complex: from genesis to revelations. *Trends in Biochemical Sciences*, **46**(7): 608–620.

Seaman MNJ, McCaffery JM, Emr SD. 1998. A membrane coat complex essential for endosome-to-Golgi retrograde transport in yeast. *Journal of Cell Biology*, **142**(3): 665–681.

Trousdale C, Kim K. 2015. Retromer: structure, function, and roles in mammalian disease. *European Journal of Cell Biology*, **94**(11): 513–521.

Vagnozzi AN, Praticò D. 2019. Endosomal sorting and trafficking, the retromer complex and neurodegeneration. *Molecular Psychiatry*, **24**(6): 857–868.

Wen L, Tang FL, Hong Y, et al. 2011. VPS35 haploinsufficiency increases Alzheimer's disease neuropathology. *Journal of Cell Biology*, **195**(5): 765–779.

Yacov N, Kafri P, Salem Y, et al. 2020. MOSPD2 is a therapeutic target for the treatment of CNS inflammation. *Clinical and Experimental Immunology*, **201**(2): 105–120.

Yu J, Feng H, Sang Q, et al. 2023. VPS35 promotes cell proliferation via EGFR recycling and enhances EGFR inhibitors response in gastric cancer. *EBioMedicine*, **89**: 104451.

Zhang JB, Ali MY, Chong HB, et al. 2025. Oxidation of retromer complex controls mitochondrial translation. *Nature*, **641**(8064): 1048–1058.

Zhang YQ, Xia N, Hu YZ, et al. 2024. Bactericidal ability of target acidic phospholipids and phagocytosis of CDC42 GTPase-mediated cytoskeletal rearrangement underlie functional conservation of CXCL12 in vertebrates. *Science China Life Sciences*, **67**(12): 2713–2729.

Zouiouich M, Di Mattia T, Martinet A, et al. 2022. MOSPD2 is an endoplasmic reticulum-lipid droplet tether functioning in LD homeostasis. *Journal of Cell Biology*, **221**(6): e202110044.